Journal of Solid State Chemistry 184 (2011) 2678–2682

Contents lists available at ScienceDirect

Journal of Solid State Chemistry

journal homepage: www.elsevier.com/locate/jssc

Growth and characterization of Cl-doped ZnO hexagonal nanodisks

Ramin Yousefi [a,*], A.K. Zak [b], M.R. Mahmoudian [c]

[a] Department of Physics, Masjed-Soleiman Branch, Islamic Azad University (I.A.U.), Masjed-Soleiman, Iran
[b] Low Dimensional Material Research Center, Department of Physics, University of Malaya, Kuala Lumpur 50603, Malaysia
[c] Department of Chemistry, University of Malaya, Kuala Lumpur 50603, Malaysia

ARTICLE INFO

Article history:
Received 14 March 2011
Received in revised form
24 July 2011
Accepted 1 August 2011
Available online 9 August 2011

Keywords:
Cl-doped ZnO nanodisks
Undoped ZnO microdisks
Anionic doping
Photoluminescence
Raman

ABSTRACT

Cl-doped ZnO nanodisks were grown on a Si(111) substrate using a thermal evaporation method. The prepared nanodisks exhibited a hexagonal shape with an average thickness of 50 nm and average diagonal of 270 nm. In addition, undoped ZnO disks with hexagonal shape were grown under the same conditions, but the sizes of these undoped ZnO disks were on the micrometer order. A possible mechanism was proposed for the growth of the Cl-doped ZnO nanodisks, and it was shown that the Cl^{1-} anions play a crucial role in controlling the size. X-ray diffraction and Raman spectroscopy clearly showed an extension in the crystal lattice of ZnO because of the presence of chlorine. In addition, these nanodisks produced a strong photoluminescence emission peak in the ultraviolet (UV) region and a weak peak in the green region of the electromagnetic spectrum. Furthermore, the UV peak of the Cl-doped ZnO nanodisks was blueshifted with respect to that of the undoped ZnO disks.

1. Introduction

ZnO, as one of the most semiconducting materials, has a wide range of applications owing to its type of structure, electronic distribution, and polarity [1,2]. ZnO has a direct band gap of 3.37 eV and a high exciton binding energy of 60 meV, which is greater than the thermal energy at room temperature. In addition, ZnO has shown splendid and abundant nanostructure configurations that a material can form. As is well known, the impurity-doping of semiconductors with selective elements greatly affects their basic physical properties such as their morphological, electrical, optical, and magnetic properties, which are crucial for their practical application. The literature shows that much attention has been paid to cationic doping in ZnO nanostructures. On the other hand, less attention has been paid to the anionic doping effect on the morphology of ZnO nanostructures and their optical properties.

Chlorine as a halogen element could serve as an anionic dopant in ZnO. Several groups have studied the morphological, optical, and electrical properties of Cl-doped ZnO nanostructures with different morphologies [3–8]. Cui et al. [3] fabricated Cl-doped ZnO nanowires using an electrochemical method. They showed that, addition of ammonium chloride in the source materials resulted in the growth of ZnO nanowires with larger diameters but reduced lengths. They also observed that, oxygen vacancy was increased with increase of ammonium chloride concentration in the source material. In addition, Elias et al. [7] observed the effect of Cl anions on aspect ratio of ZnO nanowires, which were grown by an electrodeposition method. Moreover, electron concentration of the ZnO thin film was increased by chlorine as a donor impurity [8]. Recently, ZnO nanoplates and nanodisks have attracted special interest from many scientific researchers, because of their special morphology and potential application in the electronic and photonic devices, as well as their photocatalyst applications [9–19]. However, the growth of Cl-doped ZnO nanodisks has not yet been reported by thermal evaporation method. Therefore, growth of Cl-doped ZnO nanodisks with a high optical properties and crystalline quality, using a thermal evaporation method as a simple and particularly cost effective method can be important for the applications of optoelectronic devices.

In this work, the Cl-doped ZnO nanodisks were grown on silicon substrate using a thermal evaporation method. The effects of presence chlorine as an anionic dopant on the morphological and optical properties of the ZnO nanodisks were investigated.

2. Experimental

The growth of Cl-doped ZnO nanodisks was performed in a horizontal tube furnace. This system contained a quartz tube vacuum chamber that was 100 cm in length and 5 cm in diameter. A smaller one-ended quartz tube (50 cm in length and 2 cm in diameter) that contained the precursor materials

* Corresponding author. Fax: +986813330093.
E-mail address: yousefi.ramin@gmail.com (R. Yousefi).

0022-4596/$ - see front matter © 2011 Elsevier Inc. All rights reserved.
doi:10.1016/j.jssc.2011.08.001

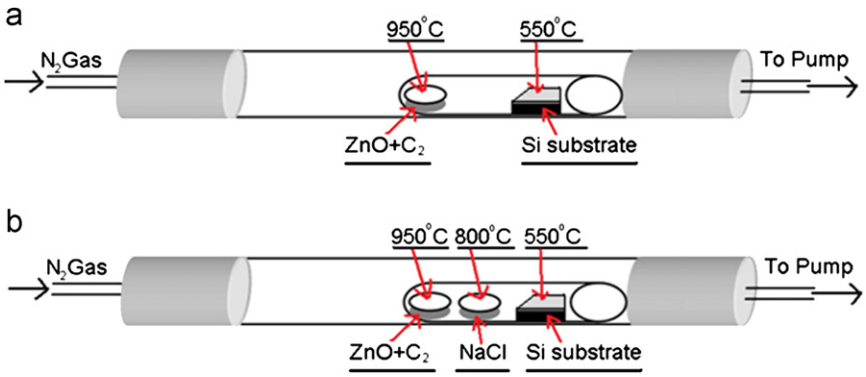

Fig. 1. Schematic of set-up used for growth of (a) undoped ZnO disks and (b) Cl-doped ZnO nanodisks.

($ZnO+C_2$ and NaCl) and substrate was placed within the vacuum chamber. First, Si(111) substrates were ultrasonically cleaned using ethanol and de-ionized water. They were then lightly etched with an HF (43%) and de-ionized water mixture (1:10) for about 10 min to remove the native oxide layer. A mixture of zinc oxide powder (99.99%) and commercial graphite powder at a 1:1 weight ratio was used as the precursor material for the ZnO, and NaCl powder (99.99%) was used for the precursor material of Cl ($Mol_{ZnO}/Mol_{NaCl}=10:2$). The precursor material for the ZnO was placed at the closed end of the smaller quartz tube, while the NaCl powder was placed 15 cm away from the ZnO material, and a Si(111) substrate was placed downstream of the precursor materials, as shown in Fig. 1. The small tube was then inserted into the vacuum chamber such that the closed end was at the center of the furnace. The ZnO and NaCl precursor materials were heated to 950 and 800 °C, respectively, and the temperature of the substrate was maintained at 550 °C during the growth process for the Cl-doped ZnO nanodisks (Fig. 1). High purity N_2 gas was fed at about 100 sccm into the furnace at one end, while the other end was connected to a rotary pump. The growth process was allowed to proceed for 1 h. A vacuum of 6 Torr was maintained inside the tube furnace during the deposition of the nanostructures. Undoped ZnO disks were also grown under the same conditions using a catalyst-free substrate.

The crystal structure and morphology of the products were investigated using a field emission scanning electron microscope (FESEM, Quanta 200 F) and an x-ray diffractometer (XRD, Siemens D5000). The elemental contents of the products were investigated using energy dispersive x-ray analysis (EDX, Quanta 200 F). Room temperature photoluminescence spectroscopy and Raman (Jobin Yvon Horiba HR 800 UV) measurements were employed to study the optical properties and crystallinity of the Cl-doped ZnO nanodisks and undoped ZnO disks. A He–Cd laser with a wavelength of 325 nm and an Ar ion laser with an emission wavelength of 514.5 nm were used for the PL and Raman measurements, respectively.

3. Results and discussion

Fig. 2(a_1) shows an FESEM image of the undoped ZnO microdisks. As can be seen, these microdisks have a wide distribution of diagonals, from 800 nm to 4 μm, with a thickness of about 1 μm and a perfect hexagonal geometry. The orientation of the microdisks growth is preferentially along the direction of the *c*-axis ([0001]), because the *c*-axis is perpendicular to the hexagonal plane. In addition, because no catalyst was used in the growth of the ZnO microdisks in this study, the vapor–liquid–solid (VLS) mechanism cannot be responsible for the growth; in fact the growth occurs via a vapor–solid (VS) mechanism. The absence of any detectable catalyst and impurity at the ZnO microdisks surface (see Fig. 2(b)) supports this statement. Fig. 2(c) shows an FESEM image of the Cl-doped ZnO nanodisks. As can also be clearly seen, the Cl-doped ZnO nanodisks have a hexagonal shape (see Fig. 2(d)), but the distribution of the diagonal of the Cl-doped ZnO nanodisks is very narrow (250–300 nm). In addition, the thickness of the Cl-doped ZnO nanodisks is on the order of several tens of nanometers (see Fig. 2(e)). Therefore, the Cl-doped ZnO nanodisks are transparent (see Fig. 2(d)). Although many of the nanodisks are stacked together, most of them lie on the substrate in a horizontal position (Fig. 2(d)), while some stand up vertically (Fig.2(e)). Fig. 2(f) and (g) shows EDX spectra of the undoped ZnO microdisks and Cl-doped ZnO nanodisks, respectively. The EDX spectrum of the Cl-doped ZnO nanodisks shows about a 6% (atomic) content for the Cl element and no peaks are detected from other materials such as Na, while the EDX spectrum in Fig. 2(f) shows that the microdisks are pure ZnO.

Fig. 3 shows XRD patterns of the undoped ZnO microdisks and Cl-doped ZnO nanodisks. The XRD patterns in Fig. 3 agree with the standard card of bulk ZnO with a hexagonal structure (JCPDS No. 800075). No peaks from Zn, Cl, or other impurities are visible. The ionic radius of the substitute Cl^{1-} ($r^1_{Cl^-}=0.18$ nm) is bigger than that of O^{2-} ($r^2_{O^-}=0.14$ nm). Thus, doping with Cl causes a slight shift in the (002) peaks toward lower diffraction angles. This shift is shown in the inset of Fig. 3. This result provides indirect evidence that chlorine is incorporated into the crystal structure, causing the ZnO crystal lattice to expand.

Raman spectroscopy is an effective technique for estimating the crystallinity of materials. According to the group theory, single crystalline ZnO belongs to the C^4_{6V} space group, with two formula units per primitive cell and eight sets of optical phonon modes at the Γ point of the Brillouin zone, classified as $A_1+E_1+2E_2$ modes (Raman active), $2B_1$ modes (Raman silent) and A_1+E_1 modes (infrared active). The E_1 and A_1 modes are two polar modes and are split into transverse optical (TO), and longitudinal optical (LO) branches. The Raman spectra for the undoped ZnO microdisks and Cl-doped ZnO nanodisks are presented in Fig. 4. The two samples exhibit a similar scattering peaks, indicating that they have identical crystal structures, as confirmed by the XRD patterns. As shown in Fig. 4, the Raman spectra show sharp, strong, and dominant peaks at 437 cm^{-1} and 438.1 cm^{-1} for the undoped ZnO microdisks and Cl-doped ZnO nanodisks, respectively, corresponding to the E_2(high) mode of the Raman active mode, a characteristic peak for the wurtzite hexagonal phase of ZnO. In addition, the E_2(high) peak in the Cl-doped ZnO nanodisks shows a blueshift of 1.1 cm^{-1} compared to the ZnO microdisks (see the inset of Fig. 4). This shift in the E_2(high) peak of the Raman spectrum is usually used to determine the biaxial stress in ZnO nanostructures [20]. The E_2(high) mode of the wurtzite ZnO crystal would shift to a higher frequency under a biaxial compressive stress within the *c*-axis oriented ZnO

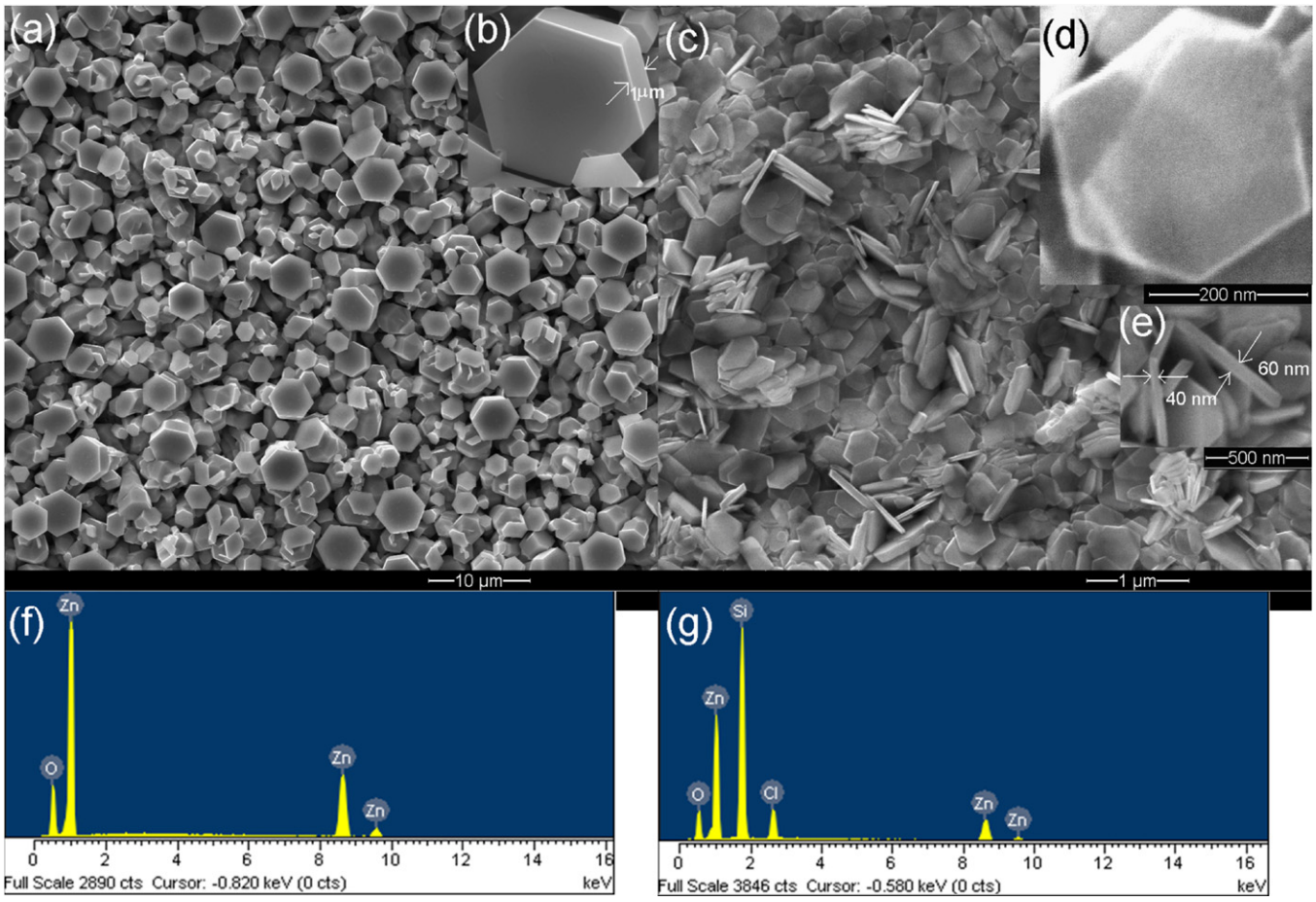

Fig. 2. (a) Low magnification FESEM image of undoped ZnO microdisks, (b) high magnification FESEM image of single undoped ZnO microdisk, (c) low magnification FESEM image of Cl-doped ZnO nanodisks, (d) high magnification FESEM image of single Cl-doped ZnO nanodisks, (e) vertical Cl-doped ZnO nanodisks with thicknesses in nanometer range, (f) EDX spectrum of undoped ZnO microdisks and (g) EDX spectrum of Cl-doped ZnO nanodisks.

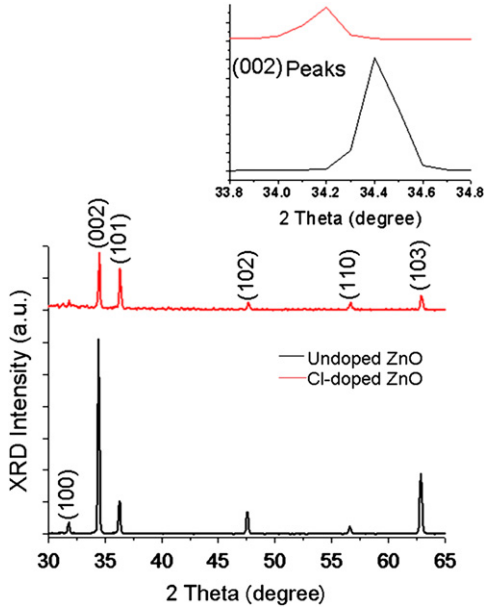

Fig. 3. XRD patterns of undoped ZnO microdisks and Cl-doped ZnO nanodisks. The inset shows the shift in the (002) peak of the Cl-doped ZnO nanodisks toward lower angles.

epilayers by

$$\Delta\omega\ (\mathrm{cm}^{-1}) = 4.4\sigma\ (\mathrm{GPa}) \quad (1)$$

where σ (in the direction of the c-axis) and $\Delta\omega$ are the stress in the Cl-doped ZnO nanodisks in GPa and the shift in the E_2(high) mode in cm^{-1}, respectively [21]. The blueshift of the E_2(high) mode corresponding to 437 cm^{-1} in the bulk crystal demonstrates that the Cl-doped ZnO nanodisks are under compressive stress, which is estimated to be 0.25 GPa. This result is consistent with the observed lattice expansion from the XRD measurements. In addition, Fig. 4 shows two peaks at 331 cm^{-1} and 378 cm^{-1}, assigned to the E_{2H}–E_{2L} (multi-phonon process) mode and A_1(LO), respectively, for both samples. The E_{2H}–E_{2L} can only be found when the ZnO is a single crystal [22]. A weak peak at 579 cm^{-1} corresponding to E_1(LO) is indicated for both samples. The E_1(LO) mode is associated with impurities and formation defects such as oxygen vacancies [23]. Therefore, the appearance of negligible E_1(LO) peaks for both samples indicates a higher crystalline quality and lower oxygen vacancy for them.

It is known that diffusion will occur even if the total pressure is constant and uniform inside the tube, as long as there is a spatial difference in the chemical potential. Such a potential is normally represented by the difference in the concentrations or partial pressures of the compounds in a gas mixture. Because of this, the ZnO and NaCl vapors can propagate toward the substrate

in our configuration. Therefore, the growth process of the undoped ZnO microdisks can be explained by the following reactions:

$$ZnO(s)+C(s)\rightarrow Zn(g)+CO(g) \quad (2)$$

$$ZnO(s)+CO(g)\rightarrow Zn(g)+CO_2(g) \quad (3)$$

$$Zn(g)+CO(g)\rightarrow ZnO(\text{microdisks})+C(s) \quad (4)$$

In fact, graphite was introduced into the raw materials to reduce the oxides into metals, as shown in reaction (2). Moreover, the sublimed Zn atoms are carried downstream by the diffusion process, and in the lower-temperature region, Zn atoms condense and form liquid clusters, which tend to deposit fairly uniformly onto the silicon substrate. The liquid droplets quickly solidify on the substrate in the deposition temperature zone. From a surface-energy point of view, the lowest energy facets for Zn are {0001}, and then $\{10\bar{1}0\}$ and $\{2\bar{1}\bar{1}0\}$. Thus, faceted, single crystalline Zn hexagonal disks tend to form, which are enclosed by {0001} top and bottom surfaces and $\{10\bar{1}0\}$ side surfaces, as shown in Fig. 5. Considering the lower local growth temperature, the residual oxygen in the growth chamber is likely to oxidize the surface of the Zn nanodisks, but the degree to which the disks are oxidized depends on the local temperature and amount of oxygen in chamber. On the basis of the information that we gathered, a growth process for the hexagonal nanodisks can be proposed. If the (0002) facet of the crystallized ZnO is constantly kept clean and the newly incoming droplets can constantly wet and cover the entire condensed (0002) facet, the ZnO nanodisks with a geometrical shape of hexagonal projections can be obtained [24]. In our experimental conditions, the mobility of the Zn atoms in the vapor was high enough to form flat (0002) surfaces, which prevented the accumulation of incoming atoms or molecules [25]. The smooth surface of the disk, as shown in the SEM image in Fig. 2(b), provides the evidence for this assumption. However, one question arises here: Why were thin nanodisks obtained from the sample that was doped with Cl? According to the following reactions:

$$NaCl(s)\rightarrow NaCl(g) \quad (5)$$

$$Zn(g)+xCO(g)+2xNaCl(g)+1/2O_2\rightarrow ZnO_{(1-2x)}Cl_{2x}\ (\text{nanodisks}) + xNa_2CO_3 \quad (6)$$

some of the oxygen in the chamber serves to generate xNa_2CO_3 and Cl substitutes for oxygen during the oxidation of the Zn. Therefore, the lower oxidation of the Zn droplets during the growth of the Cl-doped ZnO disks causes the Cl-doped ZnO disks to be smaller than the undoped disks. Thus, we infer that the Cl^{1-} may serve as a surface-passivating agent in the reaction system. Because the ZnO crystal is a polar material in nature with a (0001) surface terminated by Zn^{2+} ions, the opposite ions (Cl^{1-}) would be adsorbed by charge compensation. The adsorption of Cl^{1-} on the Zn^{2+} terminated faces resulted in the redistribution of the surface energy and the growth rates of the different facets changed. The growth process took place at the interface of the Zn terminated facets by the combination of Cl^{1-}. Accordingly, the intrinsic growth of ZnO along the [0001] direction is substantially suppressed forming the ZnO nanodisks. Therefore, we believe that Cl^{1-} ions act as a passivation agent by charge compensation and slow the growth of ZnO along the [0001] direction, leading to the formation of Cl-doped ZnO hexagonal nanodisks (Fig. 5(c)). Xu et al. [26] also reported the effect of Cl^{1-} ions on the formation of ZnO nanodisks, which were grown using an electrodeposition method, and suggested that Cl^{1-} ions may act as a passivation agent that suppresses the growth of ZnO along the [1000] direction. In addition, this result was confirmed by Pardhan and Leung [27], who used the

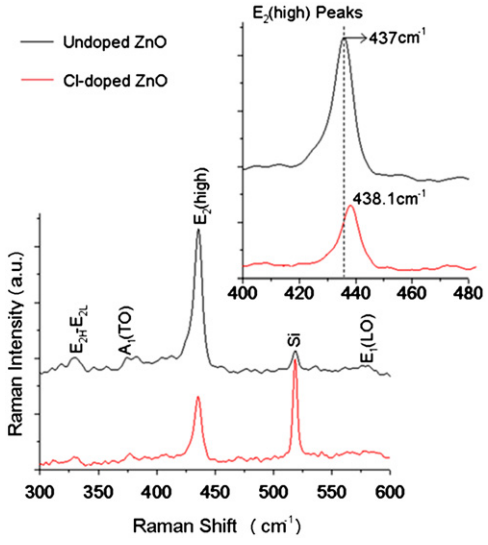

Fig. 4. Raman spectra of undoped ZnO microdisks and Cl-doped ZnO nanodisks. The inset shows a blueshift in the E_2(high) peak of the Cl-doped ZnO nanodisks.

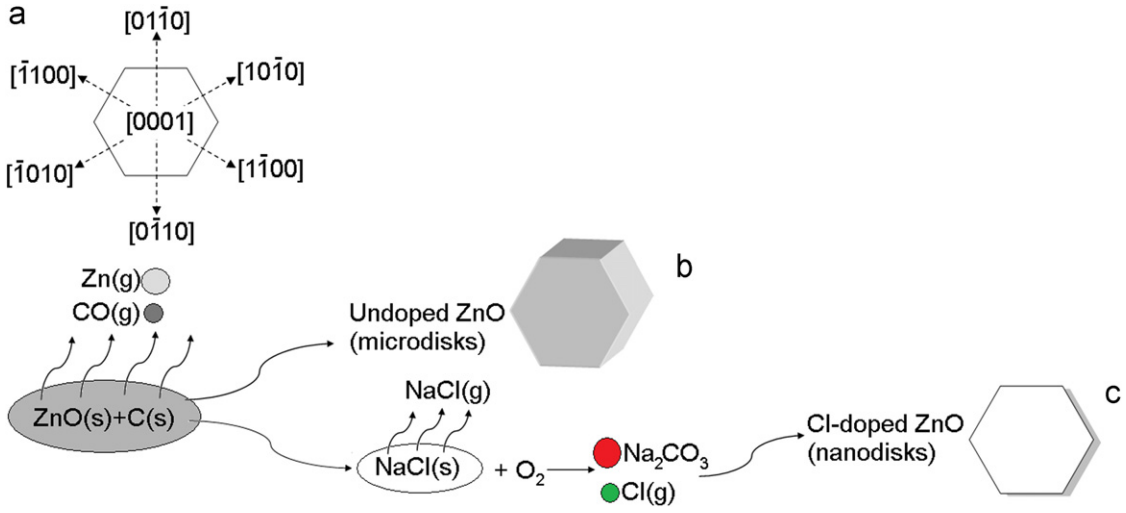

Fig. 5. (a) Isotropic epitaxial growth model of a nanodisk with hexagonal shape. Schematic diagram of proposed formation mechanisms of ZnO disk with different thickness, (b) undoped microdisk and (c) Cl-doped ZnO nanodisk.

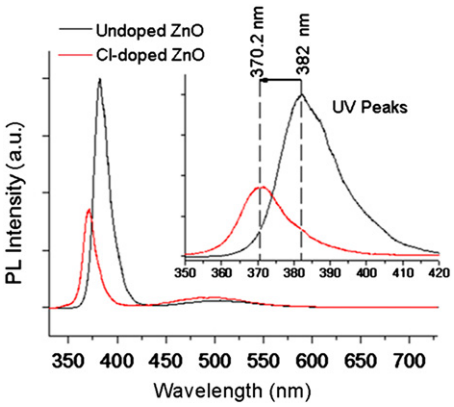

Fig. 6. PL spectra of the undoped ZnO microdisks and Cl-doped ZnO nanodisks. The inset shows a blueshift in the UV peak of the Cl-doped ZnO nanodisks.

same method to grow ZnO nanodisks. The effects of various doping elements on the formation of ZnO nanodisks have been reported using cationic dopants, including In-doped [28–31], Sn-doped [32], Pb-doped [33] and Al-doped ZnO nanodisks [18,34]. All of these cationic dopants also acted as passivation agents in the formation of ZnO nanodisks.

A PL study is a powerful method for investigating the effects of impurity doping on optical properties of ZnO nanostructures, because doped ZnO nanostructures are expected to have different optical properties in comparison with undoped ZnO. Fig. 6 shows the room temperature PL spectra of the undoped ZnO microdisks and Cl-doped ZnO nanodisks. Both of the PL spectra show a strong peak in the ultraviolet (UV) region (370.2–382 nm) and a negligible green emission (deep-level emission) peaks in the visible region at around 480 nm. Compared with the undoped ZnO microdisks, the PL spectrum of the Cl-doped ZnO nanodisks shows an obvious blueshift in the UV emission. This blueshift in the UV emission is believed to be a result of the Burstein–Moss effect because of the Cl doping in the ZnO nanodisks. The full width at half maximum (FWHM) of the UV peak of the Cl-doped ZnO nanodisks (17.32 nm) is bigger than that of the undoped ZnO microdisks (15.346 nm). This bigger FWHM of the UV peak of the Cl-doped nanodisks can be explained by the formation of band tiling in the band gap, which is often induced by the introduction of impurities into semiconductors. In addition, the UV to DLE peak ratio is one of the main factors that usually uses for comparing the optical properties of samples. The UV/DLE ratios of the Cl-doped ZnO nanodisks and undoped ZnO microdisks are about 9.5 and 24, respectively. This indicates that the undoped ZnO microdisks have a better relative crystalline quality. The lower optical quality of the Cl-doped ZnO nanodisks in comparison with the undoped ZnO microdisks could be because of the biaxial stress of the Cl-doped ZnO nanodisks, which was shown by the Raman results. As is known, biaxial stress can decrease the crystalline and optical qualities of a sample [35].

4. Conclusion

The thermal evaporation method was used to grow Cl-doped ZnO nanodisks and undoped ZnO microdisks. It was observed that, the Cl^{1-} played an important role at the Zn^{2+}(0001) surface of ZnO in the formation of nano-size ZnO disks. A shift in the (002) peak of the XRD pattern and the E_2(high) peak of the Raman spectrum indicated that the Cl-doped ZnO nanodisks structure was under a biaxial stress because of the presence of chlorine. The UV peak of the PL spectrum was blueshifted for the doped sample. This indicated that the Cl^{1-} doping induced the Burestin–Moss effect and band gap widening in the ZnO nanodisks. In addition, the PL results showed that the crystalline and optical qualities of the ZnO nanodisks were reduced by Cl doping.

Acknowledgment

Authors would like to thank Prof. Dr. M.R. Muhamad from Low Dimensional Materials Research Center, Department of Physics, University of Malaya for his support in this work. In addition, R. Yousefi gratefully acknowledges Masjed-Soleiman Branch, Islamic Azad University, for its support in this research work.

References

[1] R. Yang, Y. Qin, C. Li, L. Dai, Z.L. Wang, Appl. Phys. Lett. 94 (2009) 022905.
[2] Z.L. Wang, Adv. Funct. Mater. 18 (2008) 1.
[3] J.B. Cui, Y.C. Soo, T.P. Chen, J. Phys. Chem. C 112 (2008) 4475.
[4] Z. Tao, X. Yu, X. Fei, J. Liu, G. Yang, Y. Zhao, S. Yang, L. Yang, Opt. Mater. 31 (2008) 1.
[5] Z. Tao, X. Yu, X. Fei, J. Liu, L. Yang, S. Yang, Mater. Lett. 62 (2008) 1187.
[6] E. Chikoidze, M. Modreanu, V. Sallet, O. Gorochov, P. Galtier, Phys. Status Solidi (a) 205 (2008) 1575.
[7] J. Elias, R. Tena-Zaera, C. Le´vy-Cle´ment, J. Phys. Chem. C 112 (2008) 5736.
[8] E. Chikoidze, M. Nolan, M. Modreanu, V. Sallet, P. Galtier, Thin Solid Films 516 (2008) 8146.
[9] S.Y. Gao, H.D. Li, J.J. Yuan, Y.A. Li, X.X. Yang, J.W. Liu, Appl. Surf. Sci. 256 (2010) 2781.
[10] J.S. Jang, C.J. Yu, S.H. Choi, S.M. Ji, E.S. Kima, J.S. Lee, J. Catal. 254 (2008) 144.
[11] F. Xu, Z.Y. Yuan, G.H. Du, M. Halasa, B.L. Su, Appl. Phys. A 86 (2007) 181.
[12] B. Cao, W. Cai, J. Phys. Chem. C 112 (2008) 680.
[13] Z. Jing, J. Zhan, Adv. Mater. 20 (2008) 4547.
[14] Q. Ahsanulhaq, J.H. Kim, N.K. Reddy, Y.B. Hahn, J. Ind. Eng. Chem. 14 (2008) 578.
[15] C.X. Xu, X.W. Sun, Z.L. Dong, M.B. Yu, Appl. Phys. Lett. 85 (2004) 3878.
[16] N. Wang, H. Lin, J. Li, L. Zhang, X. Li, J. Wu, C. Lin, J. Am. Ceram. Soc. 90 (2007) 635.
[17] J. Zhang, H. Liu, Z. Wang, N. Ming, Appl. Phys. Lett. 90 (2007) 113117.
[18] J. Liu, L. Xu, B. Wei, W. Lv, H. Gao, X. Zhang, Cryst. Eng. Commun. (2010 : [18].).
[19] P.X. Gao, C.S. Lao, Y. Ding, Z.L. Wang, Adv. Funct. Mater. 16 (2006) 53.
[20] S. Tripathy, S.J. Chua, P. Chen, Z.L. Maio, J. Appl. Phys. 92 (2002) 3503.
[21] F. Decremps, J.P. Porres, A.M. Saitta, J.C. Chervin, A. Polian, Phys. Rev. B 65 (2002) 092101.
[22] A. Umar, Y.B. Hahn, Appl. Phys. Lett. 88 (2006) 173120.
[23] Y.J. Xing, Z.H. Xi, Z.Q. Xue, X.D. Zhang, J.H. Song, R.M. Wang, J. Xu, Y. Song, S.L. Zhang, D.P. Yu, Appl. Phys. Lett. 83 (2003) 1689.
[24] Z.R. Dai, Z.W. Pan, Z.L. Wang, Adv. Funct. Mater. 13 (2002) 9.
[25] Z.R. Dai, Z.W. Pan, Z.L. Wang, J. Phys. Chem. B 106 (2002) 902.
[26] L. Xu, Y. Guo, Q. Liao, J. Zhang, D. Xu, J. Phys. Chem. B 109 (2005) 13519.
[27] D. Pradhan, K.T. Leung, J. Phys. Chem. C 112 (2008) 1357.
[28] B. Aleman n, P. Ferna ndez, J. Piqueras, J. Cryst. Growth 312 (2010) 3117.
[29] J. Zhao, X. Yan, Y. Yang, Y. Huang, Y. Zhang, Mater. Lett. 64 (2010) 569.
[30] P.F. Lin, C.Y. Ko, W.T. Lin, C.T. Lee, Mater. Lett. 61 (2007) 1767.
[31] N.V. Tuyena, N.N. Longa, T.T.Q. Hoab, N.X. Nghiac, D.H. Chiad, K. Higashimined, T. Mitanid, T.D. Canha, J. Exp. Nanosci. 4 (2009) 243.
[32] Y. Ortega, P. Fernandez, J. Piqueras, Nanotechnology 18 (2007) 115606.
[33] D. Chu, Y. Zeng, D. Jiang, Mater. Res. Bull. 42 (2007) 814.
[34] X. Qu, D. Jia, Mater. Lett. 63 (2009) 412.
[35] Y. Zhang, H. Jia, R. Wang, C. Chen, X. Luo, D. Yu, Appl. Phys. Lett. 83 (2003) 4631.